Electrochimica Acta 472 (2023) 143414

Contents lists available at ScienceDirect

Electrochimica Acta

journal homepage: www.journals.elsevier.com/electrochimica-acta

Transient behavior of liquid water distribution in a lung-inspired PEM fuel cell

G.M. Cabello González [a,*], Alfredo Iranzo [a,c], Pierre Boillat [b], Felipe Rosa [a,c]

[a] Departamento de Ingeniería Energética, Grupo de Termotecnia. Escuela Técnica Superior de Ingeniería. Universidad de Sevilla. Camino de los Descubrimientos s/n 41092 Sevilla, Spain
[b] Electrochemistry Laboratory and Neutron Imaging and Activation Group, Paul Scherrer Institute, Switzerland
[c] AICIA, Escuela Técnica Superior de Ingeniería. Camino de los Descubrimientos s/n. 41092, Sevilla, Spain

ARTICLE INFO

Keywords:
PEM fuel cell
Water distribution
Water transport
Neutron imaging
Purging

ABSTRACT

Water management is a crucial aspect of hydrogen fuel cell operation because inadequate management can lead to significant losses in mass transport, limitations in oxygen diffusion, and membrane durability issues. This study investigates the impact of various operational conditions on the initial formation and evolution of liquid water content and distribution, as well as water evacuation, within a lung-inspired PEM fuel cell with a 50 cm^2 active area. A series of experiments were conducted to assess the effects of cell pressure, relative humidity of the reactant (anode and cathode), temperature, and cell current density. Neutron imaging was utilized as it has been shown to be an effective technique for quantitative analysis of water distributions. The results indicate that water initially appears in the sponges located in the central region of the cathode, but due to considerable back-diffusion, water predominantly accumulates in the area of the anode channels in contact with the cathode sponges. The amount of water in the cell increases faster when the relative humidity of the cathode and anode is higher, and high pressure and low temperature also favours water accumulation. After the experiments, the design of the cathode sponge facilitates faster water evacuation compared to the anode side. Overall, this study offers valuable insights into the behaviour of water in a hydrogen fuel cell and the factors influencing its distribution.

1. Introduction

In recent years, global economic powers have reached a consensus to pursue a transition toward a carbon-free society [1–3]. Hydrogen and electricity have emerged as the primary potential energy vectors. Hydrogen, which can be produced from diverse sources such as natural gas, biomass, and water, holds significant promise as a renewable and sustainable energy resource. Its exceptional energy density allows for substantial energy storage, rendering it an ideal fuel for both transportation and stationary power generation. Furthermore, hydrogen can be efficiently converted into electrical energy using fuel cells, which boast high efficiency and produce only water as a byproduct, making them a clean and efficient technology for power generation. These attributes collectively position hydrogen as a versatile and promising energy vector for a wide array of applications, including transportation, power generation, and industrial processes. Nevertheless, the widespread adoption of hydrogen as an energy source confronts challenges, including the high cost of production and the need for infrastructure and technological advancements [4,5]. Within this context, proton exchange membrane (PEM) fuel cells are likely to play a pivotal role in future decarbonization efforts, particularly in the transportation and power generation sectors. These fuel cells produce electricity without emitting air pollutants, making them a clean and sustainable technology that complements renewable energy sources such as wind and solar power. That way, they can compensate renewable energy sources variability by providing a constant and reliable source of electricity [6]. Also, their application in electric vehicles has the potential to reduce air pollutants emissions and improve air quality, especially in urban areas [7,8]. However, the widespread adoption of PEM fuel cells still faces challenges, including their cost, the need for infrastructure and technology development, and the availability of renewable hydrogen as a fuel [9, 10]. Nonetheless, ongoing research and development efforts are expected to address these challenges and establish PEM fuel cells a central technology in the transition to a low-carbon energy system.

* Corresponding author.
E-mail address: gcabello3@us.es (G.M.C. González).

https://doi.org/10.1016/j.electacta.2023.143414
Received 6 July 2023; Received in revised form 21 September 2023; Accepted 26 October 2023
Available online 28 October 2023

Effective water management is critical in the operation of PEM fuel cells, as both performance and durability are profoundly influenced by the distribution and content of liquid water [11–13]. Water is produced at the cathode as a byproduct of the oxygen reduction reaction and can be present in liquid state inside the cell. It plays a pivotal role in enabling proton conductivity through the membrane, facilitating the transfer of protons from the anode to the cathode. However, an excessive amount of water can be detrimental as it can accumulate in the fuel cell catalyst, gas diffusion layer (GDL), and channels. Excessive water accumulation may lead to flooding, decreasing the power output or even damaging the fuel cell [9]. This occurs as water obstructs the pores used by oxygen to reach the catalyst layer and reduces catalytic sites in the membrane [14]. Conversely, insufficient water can result in membrane drying, impairing proton conductivity. It is essential to note that water is transported from the anode to the cathode via electro-osmotic drag, potentially causing anode dehydration [15,16]. Therefore, ensuring effective water management is critical for the efficient operation and durability of PEM fuel cells and stacks. Achieving this involves designing fuel cell components to facilitate the removal of water generated during the reaction while maintaining an appropriate level of water for proton conduction through the membrane. Moreover, water purging following cell shutdown is crucial in any fuel cell system operation [17], particularly in sub-zero conditions where ice formation can severely impact the durability of sensitive components [18,19]. However, it is essential to consider that excessive purging can completely dry out the membrane, creating unfavorable conditions for subsequent fuel cell system startup. Therefore, water purging is an aspect that requires in-depth investigation in the context of PEM fuel cells [20].

Most studies investigating water and heat management in PEM fuel cells rely on advanced simulation tools like 3D multiphase computational fluid dynamics to optimize cell configurations [21]. However, due to the challenge of observing the cell's internal features, experimental investigations remain relatively scarce, with a predominant focus on the steady-state operation of the system. For instance, Zhao et al. [22] conducted experimental studies on a 50 cm^2 single PEM fuel cell, performing in-situ measurements using micro-sensors in the cathode flow field plate under various conditions. Their findings indicate that the internal resistance of PEM fuel cells is significantly affected by relative humidity, as membrane dehydration can occur under high temperatures or low gas humidity. Conversely, higher gas humidity and pressure can alleviate this issue but may also cause cathode channel flooding. Therefore, effective water management is imperative for optimizing PEM fuel cell performance and prolonging membrane durability. The design of bipolar plates and the adjustment of operating conditions play pivotal roles in achieving effective water management, preventing flooding, and enhancing cell performance, particularly under high current densities [13]. Yan et al. [23]. investigated the impact of relative humidity and membrane thickness on the one-dimensional transient process of water transport in PEM fuel cells, developing a simplified model. Their results show that higher humidification leads to more uniform water content, while reduced humidity negatively affects water content distribution and response time to reach steady state. Higher humidity benefits fuel cell performance, and thinner membranes result in more uniform water content and shorter response times. Concerning the transient behaviour of liquid water, Chen et al. [24]. explored the impact of various physical parameters on the time required for water distributions to reach steady state across the membrane in a fuel cell. The results suggest that water depletion at the anode is more pronounced than at the cathode due to a higher electro-osmotic effect, and steady-state time increases with current density. A higher initial current density leads to a smaller steady-state time, while increasing the humidification parameter at the anode can enhance water depletion at the anode. Contamination at the cathode has a greater impact on water transport, resulting in more pronounced depletion in the membrane. On a larger scale, Tang et al. [25] investigated the dynamic performance of a PEM fuel cell stack through experimental tests on the commercial Nexa module. The results reveal that different stages of load variation affect the dynamic behaviours of operating conditions such as temperature, air flow rate, and current. Typical transient phenomena including undershoot/overshoot effects, charge double-layer effect, and purge effect are observed. The frequency of purge operation increases to prevent flooding, with purge time depending on the cumulative water at the anode side. Current overshoot may occur due to elevated air transport resistance, while current undershoot may not happen due to counteracting influences. Both voltage undershoot and overshoot occur due to temporary water and gas transport issues, depending on the water contents and distributions. Operating temperature responds quickly to current load and changes gradually in an arc-like profile, with no overshoot or undershoot during transience. Air flow rate changes directly in response to dynamic load demand, with the increased amount depends on internal reaction requirements and flooding intensity.

Neutron imaging is an in-situ non-destructive imaging technique that uses neutron radiation to produce high-resolution images of the internal structures of materials. This technique is valuable for studying water management in fuel cells since it enables the visualization of water distribution throughout the entire active area [26–28]. By providing water content thickness at high spatial resolution under realistic operating conditions [29–31], neutron imaging assists researchers in gaining a deeper understanding, obtaining further insights, and optimizing the performance of PEM fuel cells. It also helps in developing more efficient and durable designs [32]. Utilizing this technique, previous research on water management in commercial serpentine bipolar plates has demonstrated that the presence of liquid water in the cathode increases as the relative humidity of both anode and cathode gases at the inlet increases, aligning with expectations [27]. Notably, the impact of anode relative humidity on fuel operation was significantly less pronounced than that of cathode relative humidity. Moreover, higher humidity had a positive effect on fuel cell performance, as increased water content in the membrane-electrode assembly (MEA) resulted in reduced ohmic resistance at low current density. Conversely, at higher current densities, the cell tended to be drier due to increased gas flows and higher cell temperatures. Furthermore, accumulated water decreased as cathode stoichiometry increased since a higher cathode flow improved water removal [33].

The design of bipolar plates is crucial for effective water management in polymer electrolyte membrane fuel cells, since gas flow channel arrangement and channel sizing (the flow field design) significantly impact water accumulation. Among various design approaches, nature-inspired designs have emerged as a promising avenues for optimizing bipolar plates and enhancing fuel cell performance. In recent years, researchers have explored nature-inspired bipolar plates [34], drawing inspiration from lungs, leaves, sponges, and honeycombs. These designs have demonstrated improved water management, reduced pressure drops, and more homogeneous gas distributions [35–40]. For example, Kang et al. [41] investigated leaf-inspired designs for bipolar plates. They found that, although the designs improved the parallel pattern, none of them outperformed the commercial serpentine design in terms of power density or water removal capacity. Nasu et al. [42] conducted research on water management in a comb-shaped cathode serpentine anode cell, highlighting the importance of gas stream velocity in removing liquid water. They also found that the use of a hydrophobic GDL resulted in more uniform water distribution. Asadzade et al. [43] designed a lung-inspired pattern for a bipolar plate which improved cell performance by reducing pressure loss, achieving uniform reactant distribution, and suitable fluid velocity. Trogadas et al. [44,45] also developed a lung-inspired flow field that distributes reactants uniformly, showing a 30 % increase in power density compared to the commercial serpentine design. In a recent study, Suárez et al. [46] explored various biomimetic designs and found that incorporating foams was particularly effective in improving water management, achieving a 6.0 % higher peak power output than the reference commercial serpentine design.

Innovative research has proposed the utilization of metal foam as the

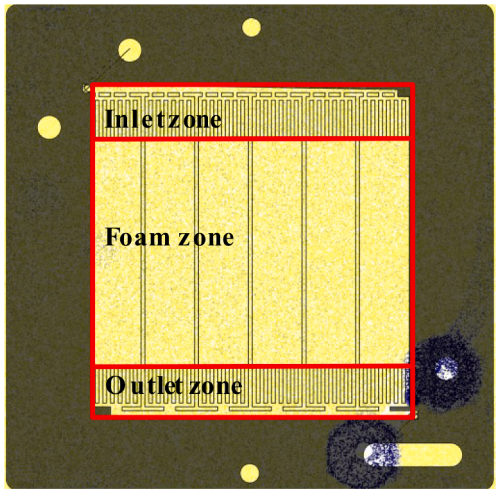

Fig. 1. Neutron imaging figure of the dry cell (not in operation) featuring the cathode design. Inlet and outlet zone correspond with a collector connected in parallel with six groups of straight channels arranged in sets of seven channels each. The foam zone comprises six areas where the graphene porous sponges are inserted. Gases enter the cathode through the upper left corner of the image and, after dispersing through the channels and passing through the foam zone, exit through the lower right corner.

flow field for bipolar plates to facilitate convective and diffusive gas flow [47]. That would lead to improved heat management and electron transport due to the high thermal and electrical conductivity of metal foams [48–51]. While this approach helps prevent water flooding, improves cold start process and enhances overall performance [52], it does raise concerns regarding the susceptibility of metal foams to corrosion and potential contamination by metal ions in membrane-electrode assemblies. To address these concerns, Chen et al. [53] introduced graphene foam combining the advantages of metal foams with the unique properties of graphene while eliminating corrosion worries. When employed as a flow field in proton exchange membrane fuel cells, graphene foam exhibited uniform reactants distribution and prevented water flooding. Also, its use improved mass transport and overall performance, particularly at high current densities [54]. Evaluation of oxygen gain, electrochemical impedance spectra, and simulations revealed that the graphene-foam MEA exhibited lower mass-transport resistance compared to conventional MEAs [55]. A study carried out by Iranzo et al. [56] analyses liquid water content and distribution in the design of Suárez et al. [46] under various operating conditions. The results indicated that high relative humidity, high pressure, low temperature, and low current density increased water content in the bipolar plates, with similar trends observed in a prior study with a different design. Furthermore, the research identified a preferential accumulation of water in the anode side, suggesting permeation from the cathode foams to the anode.

While existing literature primarily focuses on steady-state performance and water distributions within fuel cells, with limited attention to dynamic behaviour, there is a notable lack of detailed transient analysis, especially studies that consider water contents and internal water distributions. Therefore, this study aims to explore the transient process to determine the water build-up and dynamic evolution within the fuel cell, together with the analysis of the time required to reach a steady-state condition. This research also seeks insights into how water content evolves under different conditions in the novel biomimetic design proposed by Suárez et al. [46], which incorporates graphene porous sponges. The main novelty of this study lies in the application of neutron imaging to investigate transient liquid water formation and evacuation in a novel biomimetic (lung-inspired) fuel cell under various operating conditions in a quantitative manner. The concept of utilizing graphene foam in a hierarchical structure, with the main channel, sub-channels, and the porous medium in the cathode resembles the structure and function of natural systems like the trachea, bronchi, and lung alveoli. These natural systems possess a complex three-dimensional architecture comprising thin walls and a network of small channels, facilitating the exchange of gases promoting the effective transport of oxygen. In this way, graphene porous sponges and lungs share similarities in terms of their structure and functionality. Both feature a porous nature, with graphene porous sponges formed by interconnected graphene sheets and lungs composed of an intricate network of air sacs and passages. This porous composition results in a significant surface area, high gas permeability, and a notable surface area-to-volume ratio.

2. Experimental facility and methodology

2.1. Fuel cell design

The tests were conducted utilizing a bio-inspired graphite 50 cm^2 active area cell fuel, as reported by Suárez et al. [46] and [56]. As a summary, the cell comprises a cathode with an inlet and outlet collector, connected in parallel with six groups of straight channels arranged in sets of seven channels each (Fig. 1). Graphene porous sponges (density of 320 mg/cm^3 and pore size of 580 μm, Graphene Supermarket-Ronkonkoma, NY, USA) were inserted in the central area of the vertical channels. Graphene porous sponges and lungs exhibit similarities in their structure and function. They both possess a highly porous structure, with graphene porous sponges composed of interconnected graphene sheets and lungs featuring an intricate network of air sacs and passages. This porosity provides a large surface area, facilitating efficient gas diffusion. Both graphene porous sponges and lungs are involved in the exchange of gases, with the former engineered for high gas permeability. Additionally, both structures have a significant surface area-to-volume ratio, enabling enhanced gas exchange efficiency through increased interaction between gas molecules. A detailed description of the design is provided in Suárez et al. [46]. The anode is a commercial graphite serpentine flow field from ElectroChem Inc. The flow field layout is cross-flow, since the gases circulate vertically in the cathode and horizontally in the anode.

Table 1
Operating conditions defined for the set of experiments.

Test		$RH_{a,c}$ (%)	T (°C)	P (bar,g)	F_a (NmL/min)	F_c (NmL/min)	CD (A/cm^2)	Cathode feed
1	P05_T65_RH60_CD10	60	65	0.5	444	2032	1.0	air
2	P05_T65_RH90_CD10	90	65	0.5	444	2032	1.0	air
3	P10_T65_RH60_CD10	60	65	1	444	2032	1.0	air
4	P10_T65_RH90_CD10	90	65	1	444	2032	1.0	air
5	P05_T65_RH60_CD05	60	65	0.5	222	1016	0.5	air
6	P05_T65_RH90_CD05	90	65	0.5	222	1016	0.5	air
7	P10_T65_RH60_CD05	60	65	1	222	1016	0.5	air
8	P10_T65_RH90_CD05	90	65	1	222	1016	0.5	air
9	P05_T70_RH60_CD05	60	70	0.5	222	1016	0.5	air
10	P05_T55_RH60_CD05	60	55	0.5	222	1016	0.5	air

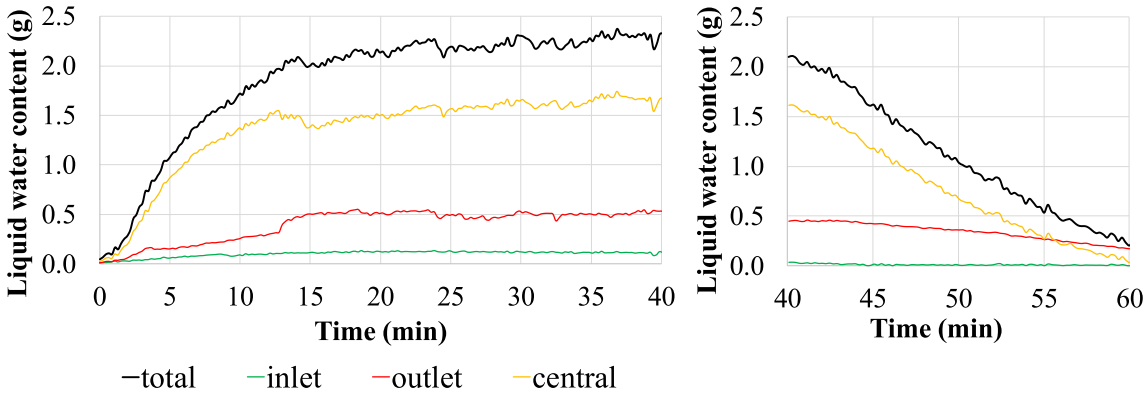

Fig. 2. Quantitative evolution of the liquid water content in the cell in Test 4 of Table 1 (P = 1 bar, T = 65 °C, RHa,c = 90 %, CD=1A/cm^2). Start up and stationary regime (left). Stop and water evacuation (right).

A GORE® PRIMEA ® MEA A510.1/M665.15/C580.4 membrane was utilized (platinum anode loading of 0.1 mg/cm^2 and cathode 0.4 mg/cm^2). Additionally, a set of Freudenberg H23C6 250 μm' thick gas diffusion layers were assembled.

2.2. Neutron imaging experimental tests

In order to study how the different operating conditions, influence the dynamics of the water distribution in the cell during the beginning and the water flush, a set of 10 experiments was carried out (Table 1). The considered operating variables were temperature, pressure, anode and cathode relative humidity, and current density, keeping constant anode and cathode stoichiometry at 1.3 and 2.5 respectively. Relative humidity was kept symmetric with the same value in the cathode and the anode ($RH_{a,c}$) in all tests. Also, air was fed to the cathode side instead of pure oxygen for every experiment. The nomenclature used to identify the tests is as follows: P11_T22_RH33_CD44, where 11 represents the operating pressure in bar with a decimal, 22 represents the operating temperature in Celsius, 33 represents the anode and cathode relative humidity in%, and 44 represents the current density in A/cm^2. Therefore, the experiment named P05_T65_RH60_CD10 corresponds to a test carried out at P = 0.5 bar, T = 65 °C, $RH_{a,c}$ = 60 %, and CD=1.0 A/cm^2.

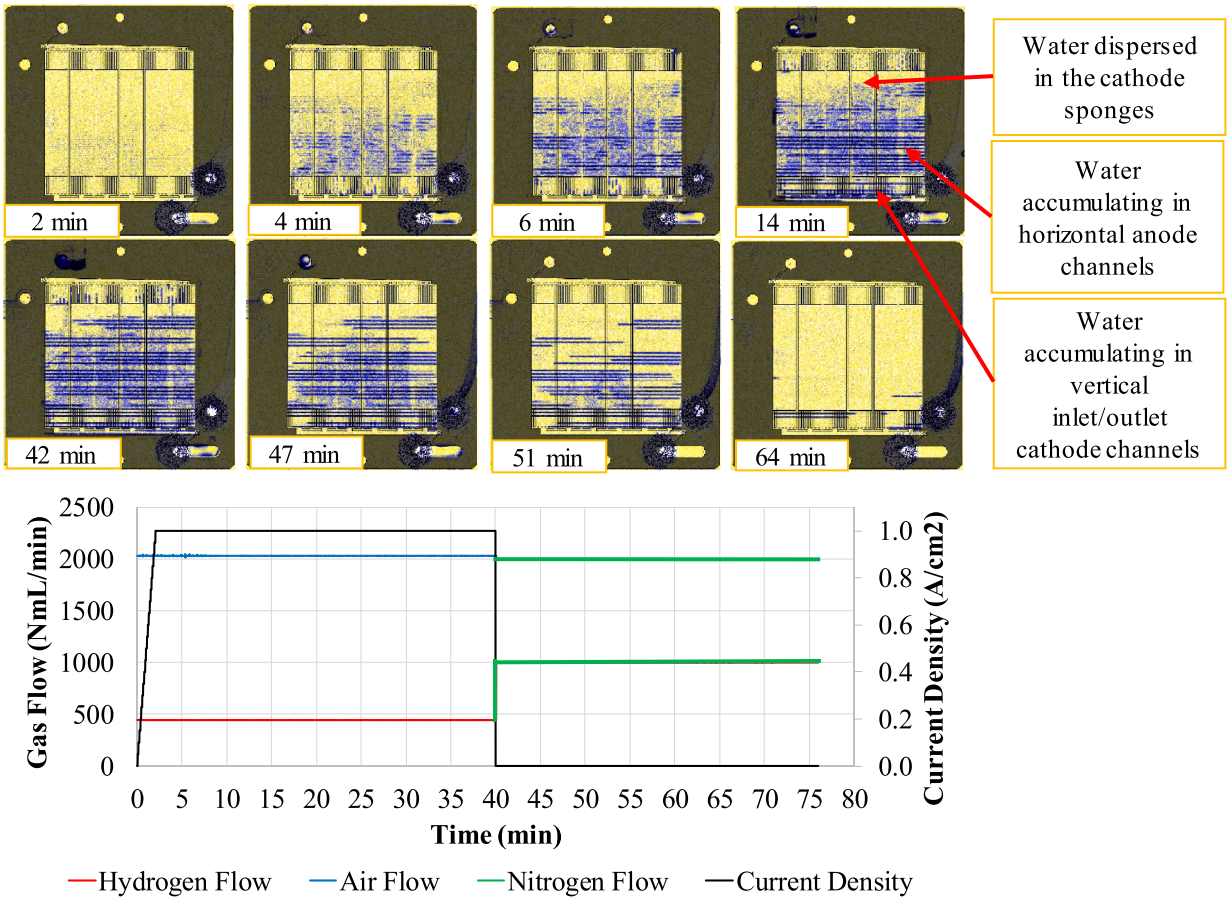

Fig. 3. Qualitative evolution of the liquid water content in the cell in Test 4 of Table 1 (P = 1 bar, T = 65 °C, RHa,c = 90 %, CD=1A/cm^2). Top: Start up and stationary regime (2–14 min), test stop and water evacuation (42–64 min). Bottom: Time evolution of gas flow rates and current density throughout the experiment.

The neutron imaging experiments followed the procedures explained in Iranzo et al. [33] and were conducted at the SINQ-NEUTRA beam-line at Paul Scherrer Institut in Villigen, Switzerland [29,30]. The experiments had a 10-second exposure time, and to ensure a fresh start for each test and prevent possible flooding effects on the GDL and MEA [28,57,58], before each test dry nitrogen was circulated through the anode and cathode during at least 20 min to dry out the cell (2 Nl/min through the cathode and 1 Nl/min through the anode), thus removing the influence of the previous tests. After the images were taken, the radiographs were corrected and pixel-wise referenced by dividing the attained images by a dry cell image to obtain the attenuation corresponding only to water. Finally, the thickness of the water was calculated using the Lambert-Beer law [27].

3. Results and discussion

This section presents the result of the neutron imaging tests carried out and the main conclusions regarding the dynamics of the water accumulation and management. Water distribution and accumulation is evaluated in every zone of the cell as well as its evacuation once the test stops. Also, the effect of changing the operating conditions in the liquid water distribution is assessed, to determine how the different operating conditions affects liquid water build up and evacuation.

In order to better investigate this, it is considered that the cell is divided into three sectors as depicted in Fig. 1. The cathode inlet and outlet regions correspond to the areas where gases enter, distribute, collect, and evacuate, while the central part is composed of the area covered by the graphene foams.

3.1. Startup process

Initial observations reveal that water initially appears in the region of the sponges inserted in the central channels of the cathode, with a tendency to condense and accumulate at the channels periphery. This phenomenon is clearly illustrated in Fig. 2 (left) and Fig. 3 (at minutes 2 and 4), presenting the results for Test 4 from Table 1 (P = 1 bar, T = 65 °C, $RH_{a,c}$ = 90 %, CD=1A/cm^2). A close-up view is presented in Fig. 3 (top right), which provides a clearer depiction of the water accumulating in the region occupied by the cathode porous sponges, cathode channels, and anode channels. Water thus appears first at the central area of the cathode side due to the reaction between oxygen molecules, protons and electrons at the cathode catalyst layer, resulting in the formation of water at the cathode side of the cell. Subsequently, water then begins to accumulate, and it's worth noting that a portion of the water from the cathode side migrates into the horizontal channels of the anode side (through back-diffusion). In these channels, the dispersed water droplets coalesce into clearly discernible water slugs in horizontal lines following the pathway of the anode flow field. Both on the anode and cathode sides, the generated water is carried towards the outlet by the gas flow. The back-diffusion effect is noticeable, particularly in the anode channels that are in contact with the cathode sponges, where water condensation occurs first. On the other hand, although liquid water is primarily generated in the central part of the cell, it tends to accumulate in the outlet region of the cell once a steady state is achieved. This is a well-known phenomenon that has already been reported previously [26]. It is a result of the joint action of gravity, since the cell is positioned vertically with the outlet at the bottom, and the drag exerted by the gases on their way to the cell outlet. In addition, inlet gases have a certain capacity to carry out water until they reach saturation, further contributing to lower water content at the cell inlet and higher content at the outlet. It's noteworthy that flooded channels presents a greater thickness of liquid water (indicated by a greater blue intensity) than the porous graphene sponges, where the water is more evenly distributed.

A study conducted by Iranzo et al. [26] investigates cross-diffusion phenomena in a cell with a serpentine flow field design both at the anode and the cathode. Another study [59] evaluates the evolution of water formation during start-up of this same design under different operating conditions. In both cases, most of the water present in the liquid state is found on the cathode side, even for inlet gas humidities of 90 %. The diffusion ow water to the anode is observed in regions devoid of water in the cathode, as it traverses the anode channels. Similar regions can also be observed in the work of Wu et al. [60] for a different serpentine configuration design. From this, it can be deduced that water crosses the membrane from one side to the other and is carried in the form of vapor within the anode channels. In contrast, the behavior observed in the biomimetic design differs, as there is a considerable amount of water in liquid form on the anode side. This difference is mainly attributable to the distinct MEA used in both studies. Iranzo et al. [26] design employ a 190-micron MEA, while the biomimetic design utilizes a significantly thinner one, measuring 20 μm. This, combined with the sponge structure in the central area of the cathode in the current design, facilitates enhanced water permeation from the cathode to the anode, resulting in a substantial presence of liquid water on the anode side.

Table 2
Time constant determined for each experiment. Water accumulation in left column (startup) and water depletion in right column (shutdown).

Test		Startup t_{63} (min)	Shutdown t_{63} (min)
1	P05_T65_RH60_CD10	10.4	47.9
2	P05_T65_RH90_CD10	6.5	50.7
3	P10_T65_RH60_CD10	9.1	50.3
4	P10_T65_RH90_CD10	7.6	52.6
5	P05_T65_RH60_CD05	11.3	58.9
6	P05_T65_RH90_CD05	11.3	–
7	P10_T65_RH60_CD05	14.1	50.3
8	P10_T65_RH90_CD05	12.1	50.7
9	P05_T70_RH60_CD05	11.3	51.6
10	P05_T55_RH60_CD05	12.6	59.2

3.2. Shutdown process

Upon completion of the test, the water is evacuated when the reactant gases are replaced with dry nitrogen that circulated through the anode and cathode to dry out the cell (2 Nl/min through the cathode and 1 Nl/min through the anode). The first area to quickly become free of water is the gases inlet zone, which empties within a few seconds as depicted in Fig. 3. The central zone, occupied by the porous foams, rapidly removes water, while the gas outlet zone takes more time to eliminate the retained liquid water. Also, the cathode quickly becomes free of condensed liquid water, whereas the water accumulated in the anode channels persists for a longer duration. This phenomenon is clearly illustrated in Fig. 3, where the remaining water after 50 min of operation is primarily present in the anode flow field channels (horizontally arranged).

Furthermore, in Fig. 2, it is evident that the shape of the curve differs between start-up and shutdown phases. During start-up, the curve can be approximated to follow a first-order system as water accumulates gradually, generated through the chemical reaction until reaching a steady state. Conversely, during the shutdown process, no further water is generated, and the accumulated water is uniformly removed by the nitrogen flow, resulting in a nearly linear decline.

3.3. Operating conditions effect

Considering that the graphs exhibit characteristics resembling a first-order system, the time constant (Table 2) has been calculated for every test. The time constant represents the duration it takes for the system's response to reach approximately 63 % of its final value. That way, it determines the rate at which the system approaches its steady state. Systems with small time constant respond rapidly to changes in input and reach its final value in a short time. Conversely, systems with a large

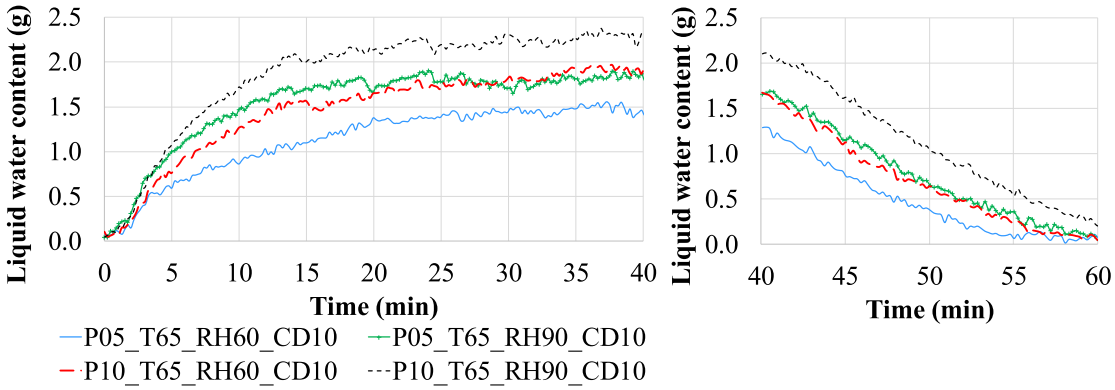

Fig. 4. Evolution of the total liquid water content in the cell for experiments carried out at a current density of 1 A/cm^2 (Tests 1, 2, 3 and 4 in Table 1).

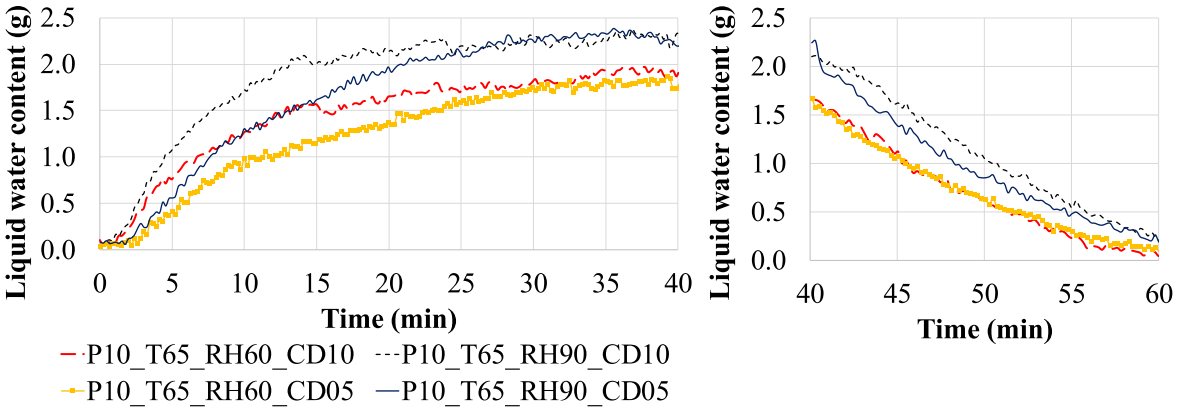

Fig. 5. Evolution of the total liquid water content in the cell for experiments carried out at 1 bar (Tests 3, 4, 7 and 8 in Table 1).

time constant respond more gradually, requiring more time to reach their final state.

In the case of experiments carried out with a current density equal to 1.0 A/cm^2 (Fig. 4), it can be observed that the total cell water content rises more rapidly when the relative humidity of both the cathode and anode is higher (experiments P05_T65_RH90_CD10 and P10_T65RH_90_CD10). Additionally, pressure seems to favor water accumulation since once the steady-state is reached, experiment 2 at 0.5 bar(g) and experiment 3 at 1.0 bar(g) show similar amounts of liquid water despite the fact that experiment 3 (at higher pressure) have significantly lower relative humidity.

It is also interesting to observe how, although higher pressure promotes water accumulation, this effect takes longer to manifest compared to other operating variables such as the relative humidity of inlet gases. At the start of the experiment, the water accumulation rate, represented by the slope of the curve, is higher for experiment 2 at 0.5 bar(g) and 90 % RH, which reaches steady-state conditions before experiment 3 (1.0 bar(g) and 60 % RH). Considering that water generation by the electrochemical reaction is the same in both experiments, this implies that the introduction of humidified gases and subsequent condensation within the cell occurs more rapidly than the water accumulation caused by higher operating pressure.

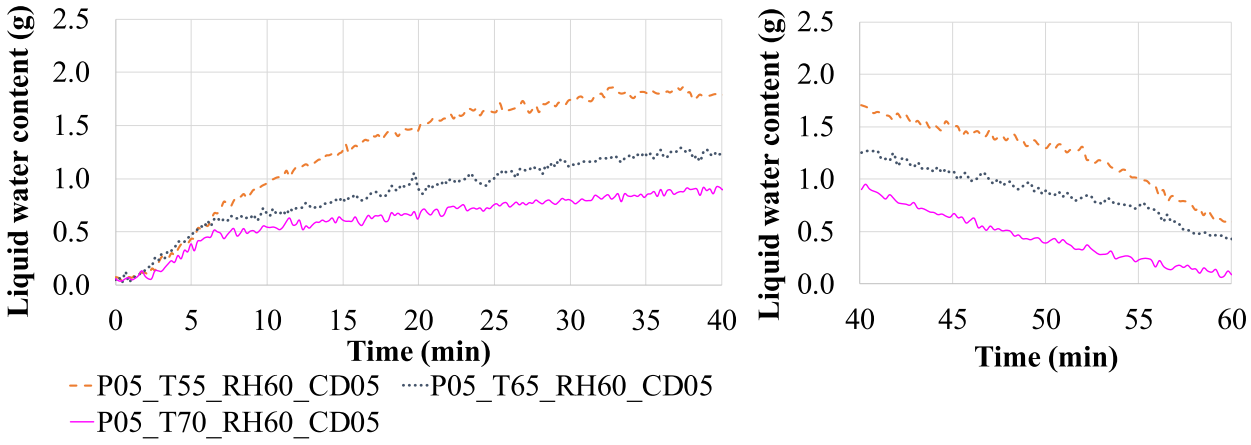

Fig. 6. Evolution of the total liquid water content in the cell for experiments carried out at 55, 65 and 70 °C. (Tests 5, 9 and 10 in Table 1).

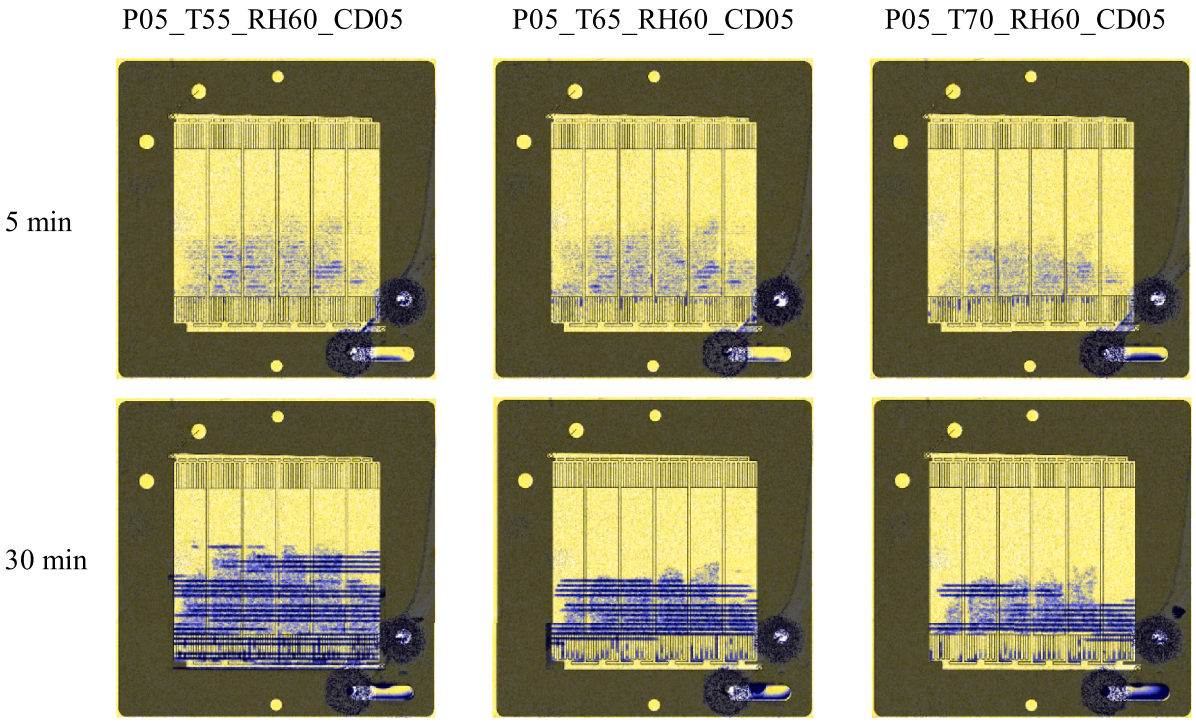

Fig. 7. Qualitative evolution of the total liquid water content in the cell at 5 and 30 min of the test for experiments carried out at 55, 65 and 70 °C. (Tests 9, 5 and 10 in Table 1).

Furthermore, the P05_T65_RH90_CD10 experiment has a lower time constant of 6.5 min, followed by the P10_T65_RH90_CD10 experiment with 7.6 min. This indicates that experiments with higher reactant humidity reach steady-state more quickly, allowing for faster stability attainment under the same conditions (6.5 vs 10.4 min and 7.6 vs 9.1 min). This trend is also observed in experiments with lower current density.

Regarding water evacuation, all four curves descend with the same slope, taking more time to reach values close to zero for the experiment with the highest liquid water content in steady-state operation. In experiments carried out at constant pressure 1.0 bar(g) (Fig. 5), it can be observed that at the beginning of the experiment, higher current density experiments present a greater water accumulation rate due to increased water generation from the electrochemical reaction. However, upon reaching steady-state, the water content of the inlet gases has a greater influence on the accumulation of liquid water in the cell. At the experiment's conclusion, water is evacuated from the cell at a similar rate (same slope) for all experiments. These trends are consistent at 0.5 bar (g). Conversely, in experiments with higher current density, the time constants of the system are lower (9.1 and 7.6 min at 1 A/cm^2 compared to 14.1 and 12.1 min at 0.5 A/cm^2). This indicates that higher current densities promote the system to reach steady-state.

Cell temperature appears to have a limited effect in the initial minutes of the experiment (Fig. 6), where the slopes are very similar until minute 6–7 of operation. At this point, the slope for the lower temperature experiment significantly decreases. As can be observed, the effect of temperature does not follow a linear trend. The difference in the accumulated water content in the cell between the experiment at 55 °C and 65 °C is smaller than the difference between the experiment at 65 °C and the experiment at 70 °C (Fig. 7). This can be attributed to the temperature-dependent liquid-vapor equilibrium. Cell operating temperature is thus a critical parameter for the water management within the cell. Notably, once the experiments are completed, experiment at 55 °C and 65 °C evacuates water in a similar way, whereas experiment at 70 °C dries up more efficiently, probably because temperature helps water evaporation and its transport out of the cell. Experiments conducted by Owejan et al. [19]. on a 50 cm2 PEM fuel cell reported the presence of liquid water 240 s after initiating the air purge in a 35 °C test. This highlights the significance of temperature effects and suggests that prolonged air purges may be necessary, particularly at lower shutdown temperatures.

4. Conclusions

The study investigates the behavior of water formation and distribution in a 50 cm^2 PEM fuel cell with a biomimetic lung-inspired sponge structure in the cathode. Neutron imaging was employed to determine liquid water content and distribution through a complete set of experiments assessing the influence of pressure, reactants relative humidity, temperature and cell current density.

It was determined that liquid water primarily accumulates in the exit region of the cell due to gravitational forces and the water drag facilitated by the reactant gases. The sponge structure in the central area of the cathode enhances greater water permeation from the cathode to the anode, resulting in a considerable amount of liquid water at the central part of the anode. As expected, pressure favors water accumulation while a lower cell temperature has a significant effect on the accumulation of water.

During the start-up of the cell, water first becomes evident in the porous sponges situated within the central zone of the cathode. Then it is drawn towards the outlet by the gas stream. Also, a considerable back-diffusion effect is observed, leading to significant water condensation in areas of the anode channels in contact with the cathode sponges. The rate of water accumulation in the cell is higher when the relative humidity of the cathode and anode increases. Purging of water at the cell shut-down proved to be more effective for the novel cathode sponge system compared to the conventional serpentine flow field.

Overall, this study provides insights into the behavior of water within a hydrogen fuel cell and the factors affecting its distribution.

CRediT authorship contribution statement

G.M. Cabello González: Methodology, Validation, Formal analysis, Data curation, Visualization, Writing – original draft, Writing – review & editing. **Alfredo Iranzo:** Conceptualization, Methodology, Software, Validation, Investigation, Supervision, Project administration. **Pierre Boillat:** Data curation, Methodology, Software, Investigation. **Felipe Rosa:** Writing – review & editing, Supervision, Funding acquisition.

Declaration of Competing Interest

The authors declare that they have no known competing financial interests or personal relationships that could have appeared to influence the work reported in this paper.

Data availability

Data will be made available on request.

Acknowledgement

This work has been funded by Secretaría General de Universidades, Investigación y Tecnología, Plan Andaluz de Investigación, Desarrollo e Innovación (PAIDI 2020), Junta de Andalucía, co-funded with ERDF funds, grant number P2018_0057_AICIA, and P20_01231. Also to the grant PID2019–104441RBI00 funded by MCIN/AEI/10.13039/501100011033, co-funded with ERDF funds, and Spanish Ministry of Economy and Competitiveness (Grant UNSE15-CE2962), funded by AEI/FEDER UE.

References

[1] DOE. DOE National Clean Hydrogen Strategy and Roadmap 2022:1–121.
[2] ROAD MAP TO A US Reducing emissions and driving growth across the nation n.d.
[3] F. Cells, Undertaking H 2J. Hydrogen Roadmap Europe : a Sustainable Pathway for the European energy Transition, Publications Office, 2019, https://doi.org/10.2843/341510.
[4] J.D. Fonseca, M. Camargo, J.M. Commenge, L. Falk, I.D. Gil, Trends in design of distributed energy systems using hydrogen as energy vector: a systematic literature review, Int. J. Hydrogen Energy 44 (2019) 9486–9504, https://doi.org/10.1016/j.ijhydene.2018.09.177.
[5] Z. Abdin, A. Zafaranloo, A. Rafiee, W. Mérida, W. Lipiński, K.R. Khalilpour, Hydrogen as an energy vector, Renew Sustain Energy Rev 120 (2020), 109620, https://doi.org/10.1016/j.rser.2019.109620.
[6] M.A. Abdelkareem, K. Elsaid, T. Wilberforce, M. Kamil, E.T. Sayed, A. Olabi, Environmental aspects of fuel cells: a review, Sci. Total Environ. 752 (2021), 141803, https://doi.org/10.1016/j.scitotenv.2020.141803.
[7] G. Wang, Y. Yu, H. Liu, C. Gong, S. Wen, X. Wang, et al., Progress on design and development of polymer electrolyte membrane fuel cell systems for vehicle applications: a review, Fuel Process Technol. 179 (2018) 203–228, https://doi.org/10.1016/j.fuproc.2018.06.013.
[8] Y. Wang, D.F. Ruiz Diaz, K.S. Chen, Z. Wang, X.C Adroher, Materials, technological status, and fundamentals of PEM fuel cells – a review, Mater Today 32 (2020) 178–203, https://doi.org/10.1016/j.mattod.2019.06.005.
[9] Q. Liu, F. Lan, J. Chen, C. Zeng, J. Wang, A review of proton exchange membrane fuel cell water management: membrane electrode assembly, J. Power Sources 517 (2022), 230723, https://doi.org/10.1016/j.jpowsour.2021.230723.
[10] L. Vichard, N.Y. Steiner, N. Zerhouni, D. Hissel, Hybrid fuel cell system degradation modeling methods: a comprehensive review, J. Power Sources 506 (2021), 230071, https://doi.org/10.1016/j.jpowsour.2021.230071.
[11] X.R. Wang, Y. Ma, J. Gao, T. Li, G.Z. Jiang, Z.Y. Sun, Review on water management methods for proton exchange membrane fuel cells, Int. J. Hydrogen Energy 46 (2021) 12206–12229, https://doi.org/10.1016/j.ijhydene.2020.06.211.
[12] R. Singh, A.S. Oberoi, T. Singh, Factors influencing the performance of PEM fuel cells: a review on performance parameters, water management, and cooling techniques, Int. J. Energy Res. 46 (2022) 3810–3842, https://doi.org/10.1002/er.7437.
[13] K. Jiao, X. Li, Water transport in polymer electrolyte membrane fuel cells, Prog. Energy Combust Sci. 37 (2011) 221–291, https://doi.org/10.1016/j.pecs.2010.06.002.
[14] P.C. Okonkwo, C. Otor, A review of gas diffusion layer properties and water management in proton exchange membrane fuel cell system, Int. J. Energy Res. 45 (2021) 3780–3800, https://doi.org/10.1002/er.6227.
[15] W. Dai, H. Wang, X.Z. Yuan, J.J. Martin, D. Yang, J. Qiao, et al., A review on water balance in the membrane electrode assembly of proton exchange membrane fuel cells, Int. J. Hydrogen Energy 34 (2009) 9461–9478, https://doi.org/10.1016/j.ijhydene.2009.09.017.
[16] G. Karimi, X. Li, Electroosmotic flow through polymer electrolyte membranes in PEM fuel cells, J. Power Sources 140 (2005) 1–11, https://doi.org/10.1016/j.jpowsour.2004.08.018.
[17] Y.S. Kim, S. Kim, N.W. Lee, M.S Kim, Study on a purge method using pressure reduction for effective water removal in polymer electrolyte membrane fuel cells, Int. J. Hydrogen Energy 40 (2015) 9473–9484, https://doi.org/10.1016/j.ijhydene.2015.05.136.
[18] Q. Yan, H. Toghiani, Y.W. Lee, K. Liang, H. Causey, Effect of sub-freezing temperatures on a PEM fuel cell performance, startup and fuel cell components, J. Power Sources 160 (2006) 1242–1250, https://doi.org/10.1016/j.jpowsour.2006.02.075.
[19] J.P. Owejan, J.J. Gagliardo, J.M. Sergi, S.G. Kandlikar, T.A. Trabold, Water management studies in PEM fuel cells, Part I: fuel cell design and in situ water distributions, Int. J. Hydrogen Energy 34 (2009) 3436–3444, https://doi.org/10.1016/j.ijhydene.2008.12.100.
[20] S. Xu, B. Yin, Z. Li, F. Dong, A review on gas purge of proton exchange membrane fuel cells: mechanisms, experimental approaches, numerical approaches, and optimization, Renew Sust. Energy Rev. 172 (2023), 113071, https://doi.org/10.1016/j.rser.2022.113071.
[21] G. Zhang, K. Jiao, Multi-phase models for water and thermal management of proton exchange membrane fuel cell: a review, J. Power Sources 391 (2018) 120–133, https://doi.org/10.1016/j.jpowsour.2018.04.071.
[22] J. Zhao, Z. Tu, S.H. Chan, In-situ measurement of humidity distribution and its effect on the performance of a proton exchange membrane fuel cell, Energy 239 (2022), 122270, https://doi.org/10.1016/j.energy.2021.122270.
[23] W.M. Yan, H.S. Chu, J.Y. Chen, C.Y. Soong, F. Chen, Transient analysis of water transport in PEM fuel cells, J. Power Sources 162 (2006) 1147–1156, https://doi.org/10.1016/j.jpowsour.2006.07.047.
[24] F. Chen, Y.G. Su, C.Y. Soong, W.M. Yan, H.S Chu, Transient behavior of water transport in the membrane of a PEM fuel cell, J. Electroanal. Chem. 566 (2004) 85–93, https://doi.org/10.1016/j.jelechem.2003.11.016.
[25] Y. Tang, W. Yuan, M. Pan, Z. Li, G. Chen, Y. Li, Experimental investigation of dynamic performance and transient responses of a kW-class PEM fuel cell stack under various load changes, Appl. Energy 87 (2010) 1410–1417, https://doi.org/10.1016/j.apenergy.2009.08.047.
[26] A. Iranzo, P. Boillat, Liquid water distribution patterns featuring back-diffusion transport in a PEM fuel cell with neutron imaging, Int. J. Hydrogen Energy 39 (2014) 17240–17245, https://doi.org/10.1016/j.ijhydene.2014.08.042.
[27] A. Iranzo, P. Boillat, J. Biesdorf, E. Tapia, A. Salva, J. Guerra, Liquid water preferential accumulation in channels of PEM fuel cells with multiple serpentine flow fields, Int J. Hydrogen Energy 39 (2014) 15687–15695, https://doi.org/10.1016/j.ijhydene.2014.07.101.
[28] A. Iranzo, P. Boillat, F. Rosa, Validation of a three dimensional PEM fuel cell CFD model using local liquid water distributions measured with neutron imaging, Int. J. Hydrogen Energy 39 (2014) 7089–7099, https://doi.org/10.1016/j.ijhydene.2014.02.115.
[29] N. Kardjilov, I. Manke, R. Woracek, A. Hilger, J. Banhart, Advances in neutron imaging, Mater. Today 21 (2018) 652–672, https://doi.org/10.1016/j.mattod.2018.03.001.
[30] N. Martinez, L. Porcar, S. Escribano, F. Micoud, S. Rosini, A. Tengattini, et al., Combined operando high resolution SANS and neutron imaging reveals in-situ local water distribution in an operating fuel cell, ACS Appl. Energy Mater. 2 (2019) 8425–8433, https://doi.org/10.1021/acsaem.9b01266.
[31] A. Iranzo, J.M. Gregorio, P. Boillat, F. Rosa, Bipolar plate research using computational fluid dynamics and neutron radiography for proton exchange membrane fuel cells, Int. J. Hydrogen Energy 45 (2020) 12432–12442, https://doi.org/10.1016/j.ijhydene.2020.02.183.
[32] P. Boillat, E.H. Lehmann, P. Trtik, M. Cochet, Neutron imaging of fuel cells – Recent trends and future prospects, Curr. Opin. Electrochem. 5 (2017) 3–10, https://doi.org/10.1016/j.coelec.2017.07.012.
[33] A. Iranzo, P. Boillat, J. Biesdorf, A. Salva, Investigation of the liquid water distributions in a 50cm2 PEM fuel cell: effects of reactants relative humidity, current density, and cathode stoichiometry, Energy 82 (2015) 914–921, https://doi.org/10.1016/j.energy.2015.01.101.
[34] S. Zhang, H. Xu, Z. Qu, S. Liu, F.K. Talkhoncheh, Bio-inspired flow channel designs for proton exchange membrane fuel cells: a review, J. Power Sources 522 (2022), 231003, https://doi.org/10.1016/j.jpowsour.2022.231003.
[35] A. Ozden, M. Ercelik, D. Ouellette, C.O. Colpan, H. Ganjehsarabi, F. Hamdullahpur, Designing, modeling and performance investigation of bio-inspired flow field based DMFCs, Int. J. Hydrogen Energy 42 (2017) 21546–21558, https://doi.org/10.1016/j.ijhydene.2017.01.007.
[36] M. Karthikeyan, P. Karthikeyan, M. Muthukumar, V. Magesh Kannan, K. Thanarajan, T. Maiyalagan, et al., Adoption of novel porous inserts in the flow channel of PEM fuel cell for the mitigation of cathodic flooding, Int. J. Hydrogen Energy 45 (2020) 7863–7872, https://doi.org/10.1016/j.ijhydene.2019.08.151.
[37] M. Marappan, R. Narayanan, K. Manoharan, M.K. Vijayakrishnan, K. Palaniswamy, S. Karazhanov, et al., Scaling up studies on PEMFC using a modified serpentine flow field incorporating porous sponge inserts to observe water molecules, Molecules 26 (2021), https://doi.org/10.3390/molecules26020286.
[38] M.J. Kermani, M. Moein-Jahromi, M.R. Hasheminasab, F. Ebrahimi, L. Wei, J. Guo, et al., Application of a foam-based functionally graded porous material flow-distributor to PEM fuel cells, Energy 254 (2022), 124230, https://doi.org/10.1016/j.energy.2022.124230.

[39] T. Chen, S. Liu, L. Yang, Development of flow field plates based on asymmetric leaf structure for PEM fuel cells, Int. J. Mater Struct. Integr. 11 (2017) 229–243, https://doi.org/10.1504/IJMSI.2017.089657.
[40] H. Kahraman, A. Coban, Performance improvement of a single PEM fuel cell using an innovative flow field design methodology, Arab. J. Sci. Eng. 45 (2020) 5143–5152, https://doi.org/10.1007/s13369-020-04368-y.
[41] H.C. Kang, K.M. Jum, Y.J. Sohn, Performance of unit PEM fuel cells with a leaf-vein-simulating flow field-patterned bipolar plate, Int. J. Hydrogen Energy 44 (2019) 24036–24042, https://doi.org/10.1016/j.ijhydene.2019.07.120.
[42] M. Nasu, H. Yanai, N. Hirayama, H. Adachi, Y. Kakizawa, Y. Shirase, et al., Neutron imaging of generated water inside polymer electrolyte fuel cell using newly-developed gas diffusion layer with gas flow channels during power generation, J. Power Sources 530 (2022), 231251, https://doi.org/10.1016/j.jpowsour.2022.231251.
[43] M. Asadzade, A. Shamloo, Design and simulation of a novel bipolar plate based on lung-shaped bio-inspired flow pattern for PEM fuel cell, Int. J. Energy Res. 41 (2017) 1730–1739, https://doi.org/10.1002/er.3741.
[44] J.I.S. Cho, T.P. Neville, P. Trogadas, Q. Meyer, Y. Wu, R. Ziesche, et al., Visualization of liquid water in a lung-inspired flow-field based polymer electrolyte membrane fuel cell via neutron radiography, Energy 170 (2019) 14–21, https://doi.org/10.1016/j.energy.2018.12.143.
[45] J.I.S. Cho, T. Neville, P. Trogadas, B. Wu, D. Brett, M.O. Coppens, Nature-inspired flow-fields and water management for PEM fuel cells. Fuels petrochemicals Div 2018 - Core Program Area 2018, AIChE Annu. Meet. (2018) 74–75, https://doi.org/10.1149/ma2020-02332171mtgabs.
[46] C. Suárez, A. Iranzo, B. Toharias, F. Rosa, Experimental and numerical Investigation on the design of a bioinspired PEM fuel cell, Energy (2022), 124799, https://doi.org/10.1016/j.energy.2022.124799.
[47] K. Jiao, J. Xuan, Q. Du, Z. Bao, B. Xie, B. Wang, et al., Designing the next generation of proton-exchange membrane fuel cells, Nature 595 (2021) 361–369, https://doi.org/10.1038/s41586-021-03482-7.
[48] A. Kumar, R.G. Reddy, Materials and design development for bipolar/end plates in fuel cells, J. Power Sources 129 (2004) 62–67, https://doi.org/10.1016/j.jpowsour.2003.11.011.
[49] Y. Wu, J.I.S. Cho, M. Whiteley, L. Rasha, T.P. Neville, R. Ziesche, et al., Characterization of water management in metal foam flow-field based polymer electrolyte fuel cells using in-operando neutron radiography, Int. J. Hydrogen Energy 45 (2020) 2195–2205, https://doi.org/10.1016/j.ijhydene.2019.11.069.
[50] C.J. Tseng, B.T. Tsai, Z.S. Liu, T.C. Cheng, W.C. Chang, S.K. Lo, A PEM fuel cell with metal foam as flow distributor, Energy Convers Manag. 62 (2012) 14–21, https://doi.org/10.1016/j.enconman.2012.03.018.
[51] E. Afshari, Computational analysis of heat transfer in a PEM fuel cell with metal foam as a flow field, J. Therm. Anal Calorim. 139 (2020) 2423–2434, https://doi.org/10.1007/s10973-019-08354-x.
[52] S. Huo, L. Li, W. Shi, R. Wang, B. Lu, Y. Yin, et al., Characteristics of cold start behavior of PEM fuel cell with metal foam as cathode flow field under subfreezing temperature, Int. J. Green Energy 18 (2021) 1129–1146, https://doi.org/10.1080/15435075.2021.1891911.
[53] Z. Chen, W. Ren, L. Gao, B. Liu, S. Pei, H.M Cheng, Three-dimensional flexible and conductive interconnected graphene networks grown by chemical vapour deposition, Nat. Mater. 10 (2011) 424–428, https://doi.org/10.1038/nmat3001.
[54] J.E. Park, J. Lim, S. Kim, I. Choi, C.Y. Ahn, W. Hwang, et al., Enhancement of mass transport in fuel cells using three-dimensional graphene foam as flow field, Electrochim. Acta 265 (2018) 488–496, https://doi.org/10.1016/j.electacta.2018.01.191.
[55] J.E. Park, J. Lim, M.S. Lim, S. Kim, O.H. Kim, D.W. Lee, et al., Gas diffusion layer/flow-field unified membrane-electrode assembly in fuel cell using graphene foam, Electrochim. Acta 323 (2019), 134808, https://doi.org/10.1016/j.electacta.2019.134808.
[56] A. Iranzo, G.M. Cabello González, B. Toharias, P. Boillat, F Rosa, Water liquid distribution in a bioinspired PEM fuel cell, Int. J. Hydrogen Energy (2023), https://doi.org/10.1016/j.ijhydene.2023.08.103.
[57] J.P. Owejan, J.J. Gagliardo, S.R. Falta, T.A. Trabold, Accumulation and removal of liquid water in proton exchange membrane fuel cells, J. Electrochem. Soc. 156 (2009) B1475, https://doi.org/10.1149/1.3242295.
[58] P. Boillat, A. Iranzo, J. Biesdorf, Layer by layer segmentation of water distribution from neutron imaging of large scale cells, J. Electrochem. Soc. 162 (2015) F531–F536, https://doi.org/10.1149/2.0511506jes.
[59] A. Iranzo, A. Salva, P. Boillat, J. Biesdorf, E. Tapia, F. Rosa, Water build-up and evolution during the start-up of a PEMFC: visualization by means of Neutron Imaging, Int. J. Hydrogen Energy 42 (2017) 13839–13849, https://doi.org/10.1016/j.ijhydene.2016.11.076.
[60] Y. Wu, Q. Meyer, F. Liu, L. Rasha, J.I.S. Cho, T.P. Neville, et al., Investigation of water generation and accumulation in polymer electrolyte fuel cells using hydro-electrochemical impedance imaging, J. Power Sources 414 (2019) 272–277, https://doi.org/10.1016/j.jpowsour.2019.01.003.